AD-A056 386 SRI INTERNATIONAL MENLO PARK CA F/G 17/9
ALTAIR: AN INCOHERENT SCATTER RADAR FOR EQUATORIAL SPREAD-F STU--ETC(U)
JAN 78 R T TSUNODA, M J BARON, J OWEN DNA001-77-C-0220
UNCLASSIFIED DNA-4538T NL

1 OF 1
ADA
056386

END
DATE
FILMED
8-78
DDC

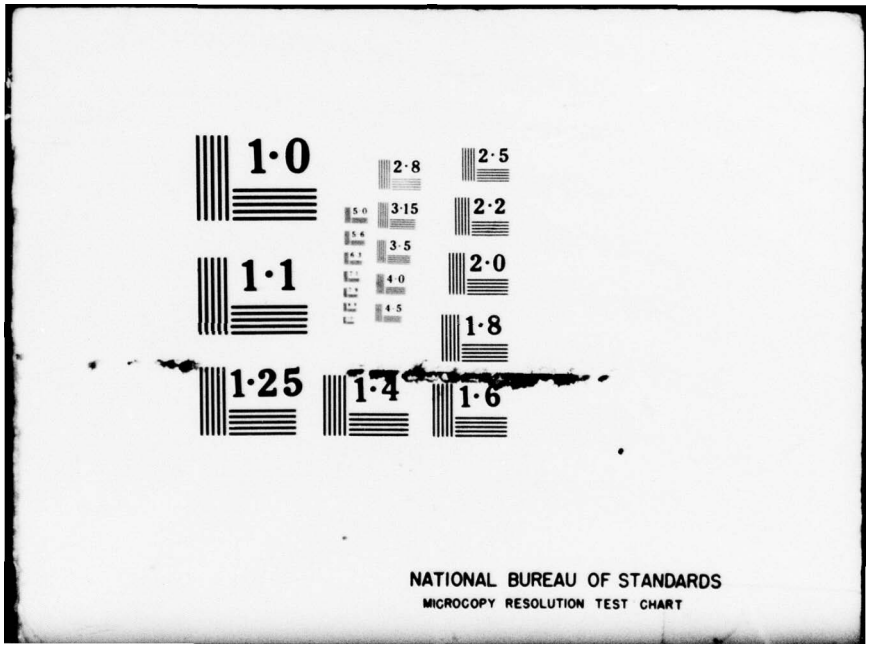
1·0
1·1
1·25
1·4
1·6
1·8
2·0
2·2
2·5
2·8
3·15
3·5
4·0
4·5
5·0
NATIONAL BUREAU OF STANDARDS
MICROCOPY RESOLUTION TEST CHART

DNA 4538T

ALTAIR: AN INCOHERENT SCATTER RADAR FOR EQUATORIAL SPREAD-F STUDIES

SRI International
333 Ravenswood Avenue
Menlo Park, California 94025

LEVEL II

January 1978

Topical Report for Period 1 June 1977—1 January 1978

CONTRACT No. DNA 001-77-C-0220

APPROVED FOR PUBLIC RELEASE;
DISTRIBUTION UNLIMITED.

THIS WORK SPONSORED BY THE DEFENSE NUCLEAR AGENCY
UNDER RDT&E RMSS CODE X322078469 Q93AAXHX63301 H2590D.

Prepared for
Director
DEFENSE NUCLEAR AGENCY
Washington, D. C. 20305

Destroy this report when it is no longer needed. Do not return to sender.

UNCLASSIFIED

SECURITY CLASSIFICATION OF THIS PAGE (When Data Entered)

REPORT DOCUMENTATION PAGE	READ INSTRUCTIONS BEFORE COMPLETING FORM
1. REPORT NUMBER: DNA 4538T	2. GOVT ACCESSION NO. / 3. RECIPIENT'S CATALOG NUMBER
4. TITLE (and Subtitle): ALTAIR: AN INCOHERENT SCATTER RADAR FOR EQUATORIAL SPREAD-F STUDIES	5. TYPE OF REPORT & PERIOD COVERED: Topical Report, 1 Jun 77—1 Jan 78
	6. PERFORMING ORG. REPORT NUMBER: SRI Project 6434
7. AUTHOR(s): R. T. Tsunoda, M. J. Baron, J. Owen	8. CONTRACT OR GRANT NUMBER(s): DNA 001-77-C-0220
9. PERFORMING ORGANIZATION NAME AND ADDRESS: SRI International, 333 Ravenswood Avenue, Menlo Park, California 94025	10. PROGRAM ELEMENT, PROJECT, TASK AREA & WORK UNIT NUMBERS: Subtask Q93AAXHX633-01
11. CONTROLLING OFFICE NAME AND ADDRESS: Director, Defense Nuclear Agency, Washington, D.C. 20305	12. REPORT DATE: January 1978
	13. NUMBER OF PAGES: 46
14. MONITORING AGENCY NAME & ADDRESS (if different from Controlling Office): DNA, SBIE	15. SECURITY CLASS (of this report): UNCLASSIFIED
	15a. DECLASSIFICATION/DOWNGRADING SCHEDULE

16. DISTRIBUTION STATEMENT (of this Report)

Approved for public release; distribution unlimited.

17. DISTRIBUTION STATEMENT (of the abstract entered in Block 20, if different from Report)

18. SUPPLEMENTARY NOTES

This work sponsored by the Defense Nuclear Agency under RDT&E RMSS Code X322078469 Q93AAXHX63301 H2590D.

19. KEY WORDS (Continue on reverse side if necessary and identify by block number)

Equatorial Spread-F
Incoherent Scatter Radar

20. ABSTRACT (Continue on reverse side if necessary and identify by block number)

In this report, we present preliminary results obtained from data collected with ALTAIR, a high-power VHF/UHF radar, during the Wideband Equatorial Program. The Wideband Equatorial Program is a coordinated field program sponsored by the Defense Nuclear Agency (DNA) to study the physical processes underlying the production of intense field-aligned irregularities and the effects of those irregularities on satellite communication channels that operate in the gigahertz frequency range. We show that this radar is sensitive enough for incoherent-scatter measurements as well as being capable

DD FORM 1 JAN 73 1473 EDITION OF 1 NOV 65 IS OBSOLETE

UNCLASSIFIED

SECURITY CLASSIFICATION OF THIS PAGE (When Data Entered)

20. ABSTRACT (Continued)

of spatially mapping E and F region irregularities as a function of time. With data collected from the operation of ALTAIR in a sector scan mode, we show that it is possible to determine the spatial distribution of 1-m spread-F irregularities and their dynamics, and to relate them to the parameters of the background equatorial ionosphere. These relationships provide a means of critically evaluating proposed source mechanisms of equatorial spread-F.

PREFACE

We gratefully acknowledge the efforts of Dr. D. M. Towle of MIT Lincoln Laboratory. Dr. Towle was instrumental in designing the ALTAIR radar experimental modes used, as well as in directing its operation during the Wideband Equatorial Program. We also thank the ALTAIR staff for their support and cooperation throughout the field experiment, and Mr. C. R. Berndtson of Lincoln Laboratory for providing the edited ALTAIR data tapes.

CONTENTS

ILLUSTRATIONS

TABLES

I. INTRODUCTION

In recent years, there has been a revival of interest in the intense, field-aligned irregularities found in the equatorial F region, now categorically known as "equatorial spread-F" irregularities (Farley et al., 1970; Balsley et al., 1972; McClure and Woodman, 1972; Farley, 1974; Balsley and Farley, 1975; Scannapieco and Ossakow, 1976; and Rottger, 1976). The impetus behind this resurgence of research activity was the surprising discovery that radio waves with frequencies in the gigahertz range can scintillate significantly when traversing a disturbed equatorial ionosphere (Crampton and Sessions, 1971; Christiansen, 1971, Craft and Westerlund, 1972). Since the current trend is to move satellite communication channels upward in frequency from the lower UHF band into the gigahertz range (where the ionospheric effects were thought to be innocuous), this discovery required serious reassessment of ionospheric irregularity characteristics and their source mechanisms. Understanding of natural processes capable of producing intense irregularities is also requisite if we intend to extrapolate these effects to communication systems operating in a nuclear environment.

Much of the progress toward understanding the production mechanism of these intense, F-region field-aligned irregularities is due to the use of the Jicamarca incoherent-scatter radar (Farley et al., 1970; McClure and Woodman, 1972; Kelley et al., 1976; Woodman and La Hoz, 1976; McClure et al., 1977; Basu et al., 1977). The principal advantage of the Jicamarca radar is continuous measurement of the electron density profile (by incoherent-scatter technique) during quiet ionospheric conditions up to the time of spread-F onset and continuous mapping of 3-m spread-F irregularities thereafter. (Because radar backscatter is obtained by Bragg scattering, the Jicamarca radar, which operates at a radar wavelength of 6 m, is sensitive to electron-density irregularities of 3-m wavelength.)

The purpose of this report is to present preliminary results of 1-m equatorial spread-F irregularities observed with ALTAIR, a high-power radar located in the equatorial zone. ALTAIR, a dedicated radar operated under the direction of the MIT Lincoln Laboratory for the U.S. Army, was recently used in support of the Wideband Equatorial Program, a coordinated satellite-rocket field experiment conducted at Kwajalein Atoll, Marshall Islands, and sponsored by the Defense Nuclear Agency. ALTAIR was operated during the field campaign for the purpose of mapping F-region field-aligned irregularities in space as a function of time.

In this report, we show that: (1) ALTAIR is sensitive enough to be operated as an incoherent-scatter radar; (2) electron density profiles can be extracted from the ALTAIR data collected during the Wideband Equatorial Program; and (3) spatial maps of spread-F irregularities obtained as a function of time provide a powerful means of studying the dynamics of those irregularities.

In Section II, we describe the radar, its mode of operation during the field experiment, and the data recorded for analysis. In Section III, we describe the data reduction procedure used to extract electron density profiles from incoherent-scatter information, and discuss the associated assumptions and limitations. Preliminary results that illustrate the kind of information available in ALTAIR data are presented in Section IV. The results are discussed in Section V in relation to other recent findings and to the collisional Rayleigh-Taylor instability, a mechanism thought to be responsible for equatorial spread-F.

II. EXPERIMENTAL CONSIDERATIONS

ALTAIR is a highly-sensitive, dual-frequency radar designed specifically to study the physical interactions between a ballistic missile in flight and its natural environment, with particular emphasis on reentry. The radar utilizes a 150-ft paraboloid antenna through which simultaneous transmissions at 155.5 and 415 MHz can be made. The antenna is fully steerable, a feature which we show to have significant value in the study of spread-F irregularities and one which is used to advantage in this study.

During the Wideband Equatorial Program, ALTAIR provided three principal support functions: (1) a means of spatial and temporal extrapolation between the Wideband satellite measurements of scintillation and in situ rocket measurements of electron density irregularities; (2) a measure of scintillation activity prior to the high-elevation passes by the Wideband satellite; and (3) high-resolution measurements of small-scale irregularity structure at VHF and UHF. The first function was accomplished by operating ALTAIR in repeated sector scans to map the distribution of spread-F irregularities in space, as a function of time. In this mode, only VHF data (i.e., 155.5 MHz) were recorded. The results reported in this report were obtained from the analysis of that data.

The sector scan data were obtained in what is called the AMTAC mode. In this mode, the antenna was steered from west to east (geomagnetic) in 21 discrete steps. Dwell time at each beam position varied between 10 and 20 s, resulting in a total scan time of 3.5 to 7 min. The AMTAC scan geometry is shown in Figure 1. ALTAIR is located on the northernmost island of Roi Namur in the Kwajalein Atoll. The scan was made in a plane oriented perpendicular to the magnetic meridian and tilted at an elevation angle of 81°. The scanned sector is shown in Figure 1 by a shaded triangle with the locations of the first, center, and last beam positions labeled by the corresponding number in the scan sequence. Also

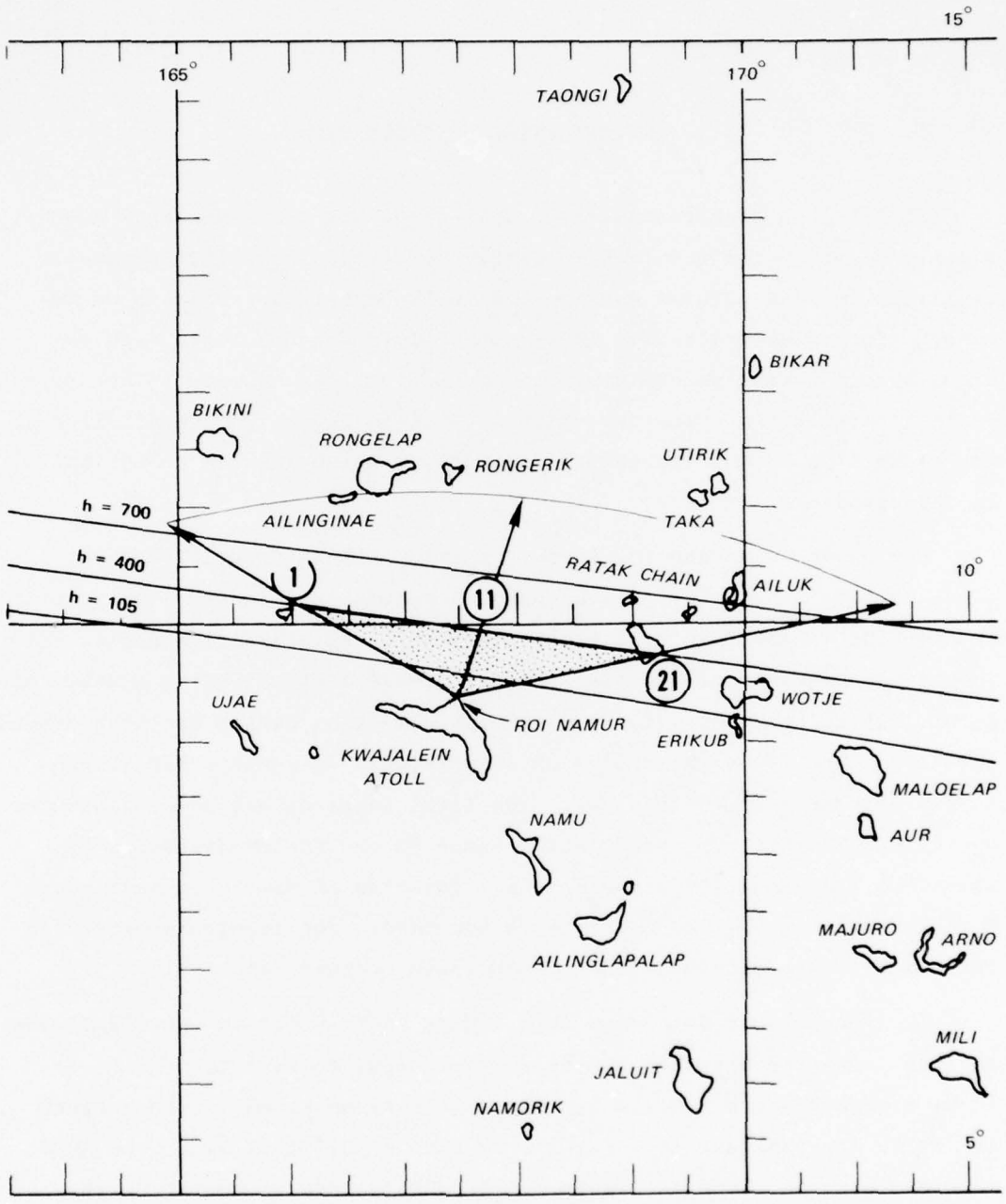

FIGURE 1 RADAR BACKSCATTER GEOMETRY FOR THE AMTAC SCAN MODE

shown are contours of exact perpendicularity between the line of sight from ALTAIR and the geomagnetic field at three different altitudes. Adjacent beam positions were separated by about 2.25^{o}, which amounted to a total scanned sector of 45^{o}.

For the AMTAC mode, only the VHF portion of the radar was used. A pulsewidth of 30 μs (4.5 km range resolution) was selected together with a pulse repetition rate of 40 s^{-1}. The received signal was detected and logarithmically amplified. Data samples were taken at 1.5-km range intervals over a 495-km extent, with a starting range that was varied according to spread-F activity. The 330 data samples were averaged over 20 transmissions (0.5 s integration in time) before being recorded on magnetic tape. In the data reduction, the number of samples were reduced to 110 by range averaging over three consecutive samples.

The data collected during the Wideband Equatorial Program are summarized in Table 1. ALTAIR was operated on eight nights in August 1977 with AMTAC data recorded during the time periods listed in the table. Some AMTAC data gaps occur within the time periods indicated because of the use of the radar for other support functions mentioned at the beginning of this section.

Table 1
ALTAIR DATA SUMMARY

Day	Date (UT)	Start Time	End Time
224	8/12/77	1053:32	1116:44
225	8/13/77	1150:45	1228:26
229	8/17/77	1016:44	1215:55
230	8/18/77	0837:23	1218:57
232	8/20/77	0817:38	1231:48
233	8/21/77	0750:24	1234:13
235	8/23/77	0815:19	1227:14
238	8/26/77	0928:20	1248:27

Before proceeding to the results, the question of the magnetic aspect sensitivity of equatorial spread-F irregularities requires some consideration, particularly if we are to interpret spatial maps of spread-F backscatter. We know that the magnetic aspect dependence of radar backscatter from auroral E-region irregularities is between 4 and 10 dB per degree (Chesnut et al., 1968; Jaye et al., 1969). Because of a much smaller collision frequency in the F region, we expect spread-F irregularities to be even more elongated along the geomagnetic field, and hence have a much steeper magnetic aspect dependence.

The magnetic-aspect angle variation over the sector scanned in the AMTAC mode is shown in Figure 2. The magnetic aspect angles were computed as a function of range for each antenna beam direction using the IGRF 1975 geomagnetic field model coefficients. Since we do not intend to make any quantitative corrections for the magnetic aspect angles, we have plotted only the results from every other beam position (labeled at the top of the pie shaped sector in Figure 2). We see that the zero magnetic aspect angle contour is located at F-region altitudes, as intended, except for a sharp deviation around beam position 9. Over the altitude range of interest (200 to 700 km), the magnetic aspect angle ranges from -0.2^{o} to $+1.0^{o}$. Therefore, we expect the spread-F backscatter maps obtained with ALTAIR probably to be significantly shaded by the magnetic aspect dependence. (This problem is less severe at Jicamarca where the dip latitude is much smaller--2^{o} compared to 9^{o} at Roi Namur. Fortunately, as shown in Section IV, the spread-F irregularity regions are generally discrete. Consequently, the qualitative morphology of these irregularity regions should not be significantly distorted.

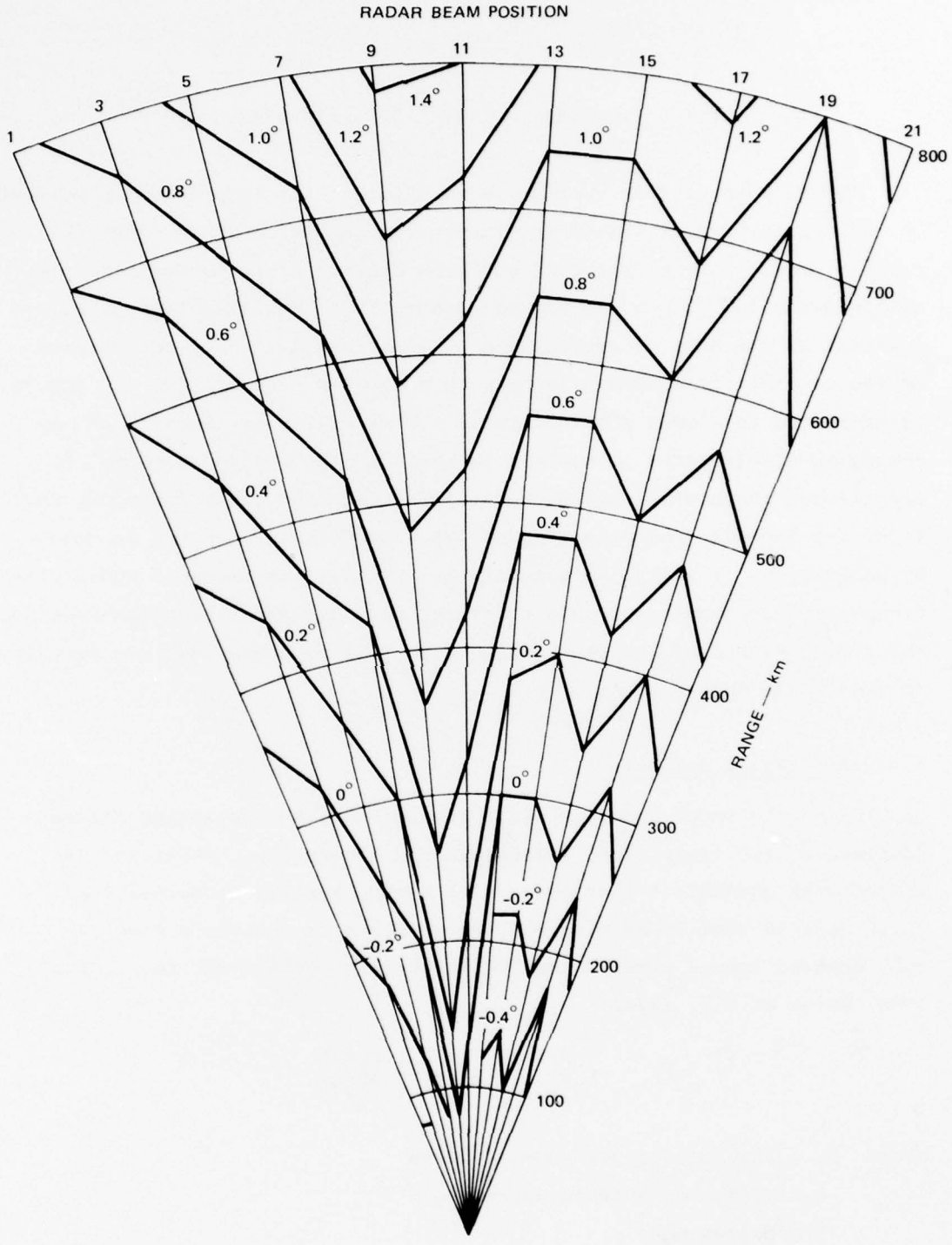

FIGURE 2 MAGNETIC-ASPECT ANGLE CONTOURS FOR THE SECTOR SCANNED IN THE AMTAC MODE

III. INCOHERENT-SCATTER DATA ANALYSIS

The purpose of this section is threefold: (1) to present an analysis of the sensitivity of ALTAIR for incoherent-scatter measurements; (2) to present preliminary examples of electron density profiles derived from ALTAIR data; and (3) to discuss the assumptions and limitations that are inherent in the data processing and interpretation. Since the purpose of the sensitivity analysis is only to establish credibility, the analysis is presented in simple physical terms. Feasibility is demonstrated by comparing ALTAIR radar parameters to those of the Chatanika radar, an operational incoherent-scatter radar. The data reduction procedure used to derive the electron density profiles is then described and followed by an example. Finally, we discuss the principal assumptions and limitations that are imposed on data collected with the radar beam intersecting the geomagnetic field at right angles, as well as those that are peculiar to the ALTAIR data set.

A. Sensitivity Analysis

Using the radar equation and assuming that the scattering volume (defined by the transmitted pulsewidth and the antenna beamwidth) is filled with equivalent scatterers each having a radar cross-section comparable to that of an electron, we obtain an approximate form for the received signal power caused by incoherent backscatter (e.g., Evans, 1969; Baron et al., 1976):

$$P_r \approx 2 \times 10^{-22} \frac{P_t A \tau N}{R^2} \qquad (1)$$

where P_t = transmitted peak power, watts
A = effective antenna aperture, m^2
τ = pulsewidth, s
N = electron density, el/m^3
R = range, m.

The noise power is given by

$$P_n = kT_s\Delta f \tag{2}$$

where $k = 1.38 \times 10^{-23}$ joules/^oK

T_s = system temperature, ^oK

Δf = system bandwidth, Hz.

The ratio of Eqs. (1) and (2) gives the signal-to-noise ratio (SNR):

$$SNR \approx \frac{15N}{R^2} \frac{P_t A\tau}{T_s \Delta f} \quad . \tag{3}$$

From Eq. (3), we see that the radar parameters of interest when determining the radar's sensitivity to incoherent backscatter are the power-aperture product (P_tA), the system noise temperature (T_s), and the pulsewidth-to-bandwidth ratio ($\tau/\Delta f$).

The radar parameters for ALTAIR and the Chatanika radar are listed in Table 2. Using the listed parameters, the power-aperture products for ALTAIR is 8.2×10^9 watts-m^2, and the Chatanika radar is 8.8×10^8 watts-m^2. That is, the signal power received by ALTAIR is 9.7 dB greater than that received by the Chatanika radar. The temperature ratio is 0.11, or -9.6 dB, favoring the Chatanika radar over ALTAIR. The final sensitivity parameter is the pulsewidth-to-bandwidth ratio. ALTAIR uses a matched-filter receiver in which the bandwidth is $1/\tau$, or for example, 33 kHz for a 30-μs pulsewidth. The Chatanika radar uses a 50-kHz bandwidth to accommodate the spectrum of the transmitted pulse as well as any Doppler effects that are prevalent in an auroral ionosphere. The ratio for ALTAIR is 9×10^{-10}s/Hz, and the ratio for the Chatanika radar is 1.34×10^{-9}s/Hz or -1.7 dB, favoring the Chatanika radar.

Table 2

COMPARISON OF RADAR SYSTEM CHARACTERISTICS

Parameter	ALTAIR	Chatanika
Frequency, MHz	155.5	1290
Peak Power, MW	10	4
Pulsewidth, μs	30	67
Antenna:		
Diameter, m(ft)	45.6 (150)	26.8 (88)
Beamwidth (deg)	2.8	0.6
Gain, dB	34.7	47.1
Effective Aperture, m^2	820	220
Temperature, ^oK	992	110
Polarization	RC/LC	RC/LC

Combining the above numbers, the SNR of ALTAIR compared to that of the Chatanika radar is

$$10 \log_{10} \left(\frac{SNR_A}{SNR_C}\right) = 9.7 - 9.6 - 1.7 \text{ dB} = -1.6 \text{ dB} \quad . \tag{4}$$

Based on the listed radar parameters in Table 2, ALTAIR is only 1.6 dB less sensitive than the Chatanika radar for incoherent-scatter measurements. However, the comparison was made with ALTAIR having approximately one-half the pulsewidth of the Chatanika radar. We therefore conclude that ALTAIR is easily capable of making incoherent-scatter measurements. (It might be of interest to note that the Jicamarca incoherent-scatter radar is approximately 8 dB more sensitive than the Chatanika radar [Evans, 1969]).

B. Electron Density Profiles

The basic data reduction procedure necessary to derive electron density profiles from incoherent-scatter data is straightforward: (1) recorded data must be time-averaged to reduce statistical variations;

(2) the mean noise power must be estimated and subtracted from the averaged data; and (3) the residual that represents the average received signal power caused by incoherent backscatter must be multiplied by a scale factor to convert signal power into electron density. The last step is usually more complicated because spectral information must be convolved into the calculations to account for variations in signal power, primarily because of variations in electron and ion temperatures (for details see Evans, 1969). Each of the above steps, however, usually differs in detail from one radar to another, depending on various factors such as radar parameters (e.g., operating frequency), desired modes of operation, and the altitude regime being sampled.

As described in Section II, the recorded data consist of 20-sample averages of the log amplitude (of the received signal-plus-noise), ordered in range, for a specific radar beam direction. Because the recorded data are already subaverages of the log amplitude, no attempt was made to "de-log" the data before further averaging. Instead, further averaging was done by direct summation of the recorded subaverages. Since we are interested in the average power, we need to know the relationship of the average of the log amplitude to the average power. We show in the Appendix that the average of the log amplitude of a Rayleigh-distributed (i.e., noiselike) signal is related to the average power by a deterministic constant. Therefore, on the assumption that the received signal was passed through a "perfect" logarithmic receiver, the averaging procedure described above should produce the desired results.

An estimate of the mean noise power is usually obtained by averaging the received power during a portion of the interpulse period that is not contaminated by signal or interference of any kind. Because of the limited range extent covered by the ALTAIR data window (495 km), a "clean" noise sample is usually not available. For our best estimate, we have selected data samples in the altitude intervals 130 to 180 km and above 450 km as the "noise" samples. The "noise" samples are probably reasonable for a quiet nighttime ionosphere when there is no F_1 layer and where the electron density above 450 km should be very small. Under disturbed conditions, the samples above 450 km can be in error by a substantial amount because of the presence of spread-F backscatter at those altitudes.

Once the mean noise power is subtracted from the averaged data, the residual must be multiplied by a scale factor that includes all constants such as the radar system constants and the relationship of the average log amplitude to average power. In principle, the scale factor can be determined directly from the data since the data is absolutely calibrated in dBsm. In practice, it is probably more reliable to determine the scale factor by using the foF2 value obtained from simultaneously recorded ionograms. Because foF2 values were not immediately available for this preliminary analysis of the data, we calculated a scale factor based on a nominal foF2 value of 8 MHz (a typical midnight equatorial ionosphere) and applied this scale factor to all data sets.

In the computation of electron density profiles from ALTAIR data, there is no compensation for temperature variations with altitude or as a function of time. This deficiency is discussed later in this section where reasonable arguments are presented that suggest that the errors introduced by this omission are acceptable for our immediate (preliminary) purposes.

An example of an electron density profile derived using the above procedure is shown in Figure 3. The data were collected on 13 August 1977 under quiet ionospheric conditions--i.e., no spread-F. These data, like all others (except for two isolated data sets), were obtained with the radar beam directed exactly perpendicular to the geomagnetic field at F-region altitudes. Therefore, actual verification that incoherent-scatter (rather than semicoherent scatter) returns are being received must await analysis of the data taken at off-perpendicular angles.

The example shown in Figure 3 represents a profile derived from data averaged over 10 s, at a fixed beam position. Several features should be noted. The profile above 200 km is very similar in shape to the nighttime equatorial F_2 layer (Bowles et al., 1963; Farley et al., 1967). We show in Section IV that profiles obtained by the above-described method are a characteristic feature in all the data and they also move in altitude and change in peak value as expected of the nighttime F_2 layer. The large spike at 105 km is a sporadic-E layer where the peak "electron density" is more likely to be a result of scattering from a gradient or electron density irregularities.

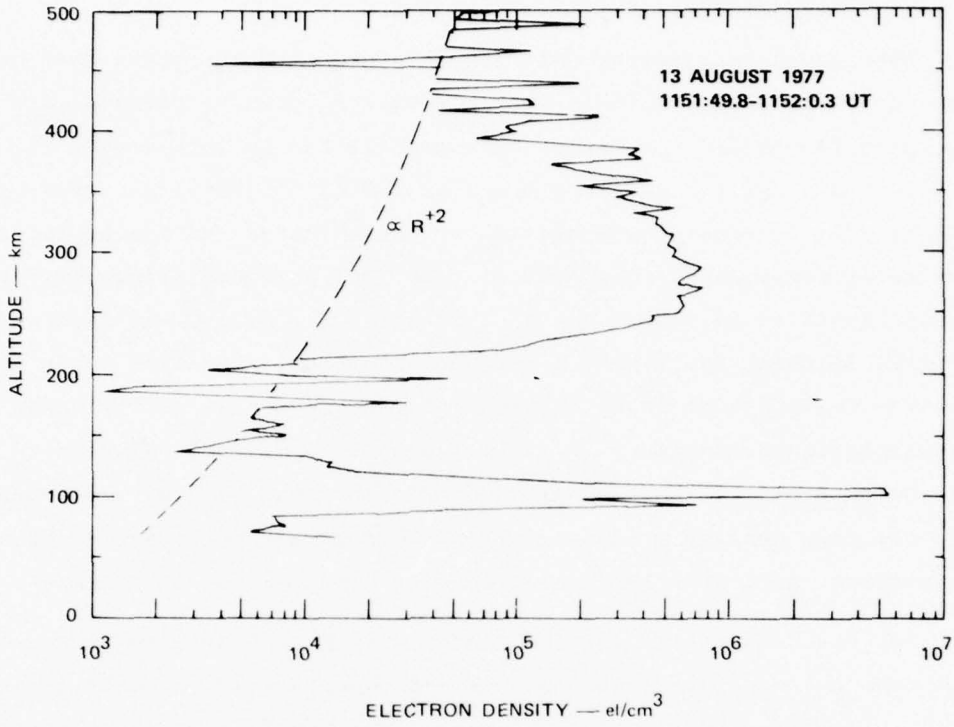

FIGURE 3 EXAMPLE OF ELECTRON DENSITY PROFILE COMPUTED FROM ALTAIR DATA

Finally, the dashed curve labeled as being proportional to range squared represents a measure of the minimum detectable signal for the integration time used. The curve actually corresponds to 1/200th the value of the mean noise power multiplied by range squared. Whenever the residual value after noise subtraction was negative, it was reassigned the above value so as to have a reasonable log plot of the profile. The large fluctuations in the profile about this curve in the altitude intervals 130 to 180 km and above 450 km is caused by the statistical nature of the data. Recall that the mean noise level itself is computed from data in these altitude intervals because no separate noise sample was taken during the operation. For the same reasons the structure in the topside of the F_2 layer seen in Figure 3 is also believed to be caused by statistical fluctuations.

C. Principal Assumptions and Limitations

When radar backscatter data are obtained with the radar beam intersecting the geomagnetic field at right angles, several effects must be accounted for before the range-power profile can be interpreted in terms of electron density. At frequencies as low as 155 MHz (that used by ALTAIR), the foremost consideration is contamination of incoherent-scatter returns by semicoherent backscatter from field-aligned irregularities. Because there is no simple way of discriminating incoherent from semicoherent returns, the system constant that relates received power to electron density must be calibrated with data taken at sufficiently large off-perpendicular angles. Any data taken at exact perpendicularity can then be interpreted in terms of incoherent-scatter returns and converted into electron density profiles. When semicoherent backscatter echoes are present, such profiles cannot be simply related to electron densities.

For the backscatter returns that are from incoherent-scatter, we must consider what other assumptions are necessary to estimate the true electron density profile from the data. It is well known that power measurements must be supplemented by spectral measurements to correct for Debye length and temperature effects. At 155 MHz, Debye length effects are entirely negligible for the electron densities of interest. Farley et al. (1967) have shown that the electron-to-ion temperature ratio (the parameter of interest) is virtually unity in the nighttime equatorial ionosphere. Since the Wideband-related operations of ALTAIR were all conducted well after sunset, there is good reason to assume that the temperature ratio is also near unity over Kwajalein.

If the temperature ratio is indeed unity, Farley et al. (1961) have shown theoretically that the total power that is backscattered is unaltered by the magnetic field. On the other hand, if the temperature ratio is not unity, Farley (1966) has shown that the total backscattered power can be enhanced up to a factor of two when the radar beam is directed normal to the geomagnetic field lines. Baron and Petriceks (1967) experimentally confirmed the theoretical results of Farley (1966). It is not clear how large an enhancement would occur using a radar with a 2.8^{o}

beamwidth. Pineo et al. (1963) found slight but negligible enhancement (relative to their experimental accuracy) when using a 425-MHz radar with a 2.2^{o} beamwidth and an 800-μs pulsewidth. Thus, we can probably neglect this effect in interpreting ALTAIR data.

IV. ONE-METER SPREAD-F IRREGULARITIES

In this section, we present examples of 1-m spread-F irregularities observed with ALTAIR operated in the AMTAC mode. Examples have been selected to illustrate the usefulness of the results for determining: (1) the spatial distribution of 1-m spread-F irregularities; (2) size, shape, and orientation of irregularity regions; (3) east-west (geomagnetic) and vertical velocities of 1-m irregularities; and (4) lifetimes of irregularity regions. The feature of particular interest in these results is the ability of the radar to measure the background electron density profile in the presence of spread-F backscatter. This feature is discussed in more detail in the following paragraphs.

Backscatter profiles from the first example are shown in Figure 4. The format of each profile is identical to the electron density profiles presented in Section III. That is, all of the backscatter profiles have been calibrated in strength as though they were caused by incoherent scatter. Hence, the profiles shown in Figure 4 (and other similar profiles to be presented in this section) are given in terms of apparent electron density, but should be interpreted as strength of backscatter above the background incoherent-scatter levels, as discussed in Section III. This format is identical to that used for the 50-MHz results from the Jicamarca radar and provides a convenient and absolute means of comparison with other results. This format and its interpretation are further clarified in following discussions.

The profiles shown in Figure 4 were taken at different beam positions during a single west-to-east scan on 23 August 1977. Conveniently, local time lags Universal time (UT) by 12 hours. Therefore, the Universal times given can be read directly as local time in the postnoon sector. The numbers in the upper right corner of each panel refer to the radar beam position. The first profile (taken at the most westward beam position) is very similar to that presented in Section III and is interpreted as

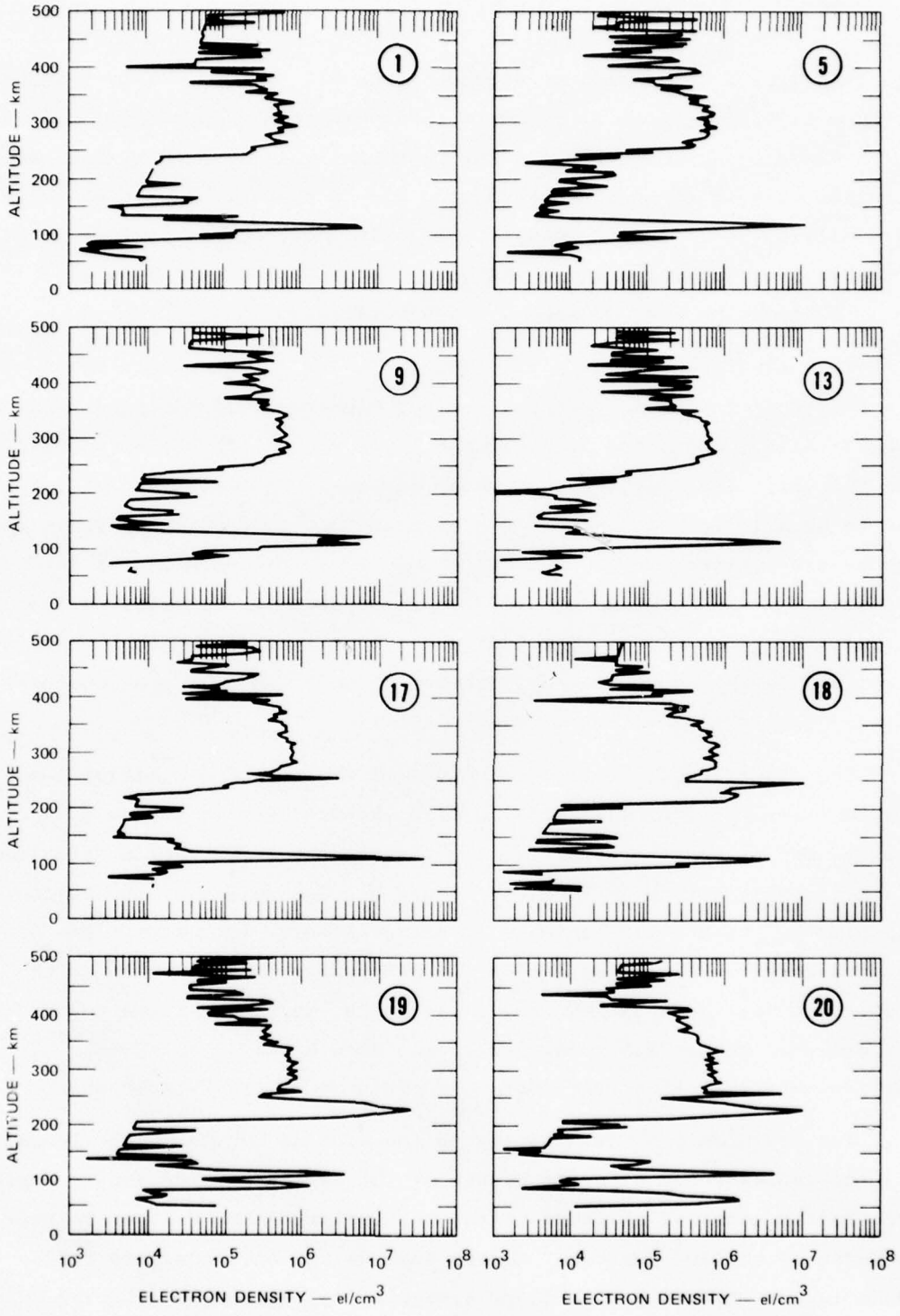

FIGURE 4 A SEQUENCE OF ALTAIR BACKSCATTER PROFILES TAKEN DURING AN AMTAC SCAN

the nighttime F layer with no spread F present. (The sporadic-E layer at approximately 100 km altitude is a feature common to all the profiles in Figure 4. Its peak value is not necessarily associated with a real electron density of that concentration and is probably caused at least partially by semicoherent backscatter.) In fact, the first four profiles are very similar, which indicates quiet conditions in the F-region ionosphere to the west of the magnetic meridian.

Examining the remaining profiles in Figure 4, which were taken near the east end of the scan, we can see the appearance of enhanced backscatter (i.e., above the background F layer values) on the bottomside of the F layer. The peak value of these spread-F echoes (beam position 19) can be seen to approach two orders of magnitude (i.e., 20 dB) above the incoherent-scatter level. A feature to note in the profiles is the stability of the background F layer. The fact that all profiles are essentially identical in shape and peak value (even those that contain spread-F) further supports our interpretation of the background profile as the mean F-layer electron density profile.

To visualize the spatial structure of the region containing 1-m spread-F irregularities associated with the profiles in Figure 4, a contour map of backscatter intensity constructed from profile data from all 21 beam positions is shown in Figure 5. The values of the contours begin at 10^5 el/cm^3 and increase in decade steps. (No attempt has been made to correct for the variation in the magnetic aspect angle in the maps. See Section II.) The small patchy 10^5 contours at the top of the map are produced by the noisiness of the data at those altitudes. The horizontal dashed line represents the altitude of the F-layer peak.

Two features are worth noting in the contour map shown in Figure 5: (1) the isolated and discrete nature of the spread-F irregularity region, and (2) the constant altitude of the bottomside of the F layer as represented by the 10^5 contour. Rather than having an ionosphere filled randomly but uniformly with these irregularity regions, we observe a single backscatter region. If they are indeed distributed as described, their spatial separations must be of the order of 200 km or more. The

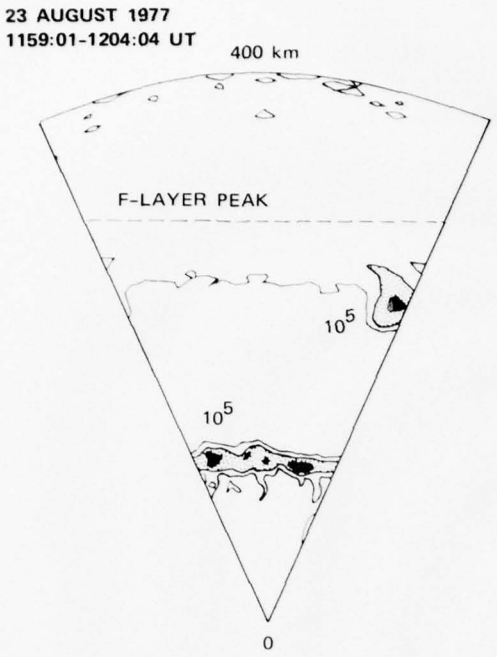

FIGURE 5 CONTOUR MAP OF ALTAIR BACKSCATTER INDENSITY CORRESPONDING TO THE BACKSCATTER PROFILES IN FIGURE 4

geometry of the irregularity region shown is that of a field-aligned rod with a transverse cross-section approximately 30 km in diameter. The altitude of the F-layer bottomside (10^5 el/cm^3 contour) is 240 km, compared to 220 km for the quiet-time profile shown in Section III. Furthermore, the bottomside gradients in the profiles shown in Figure 4 do not appear to be significantly different from the profile in Figure 3.

Another example of discrete 1-m spread-F irregularity regions is shown in Figure 6. The format is identical to that shown in Figure 5, except that the range now extends up to 500 km rather than 400 km. We have suppressed the 10^5 contour on the topside of the F layer to mask the presence of noise patches. Instead of one rod-like structure on the bottomside of the F layer, as in the previous case, we see a slab-like structure on the bottomside and a smaller rod-like structure in the topside of the F layer. The backscatter intensity from both regions are at least 10 dB greater than that in the previous example. The bottomside of the F layer is again at a virtually constant altitude in the sector west

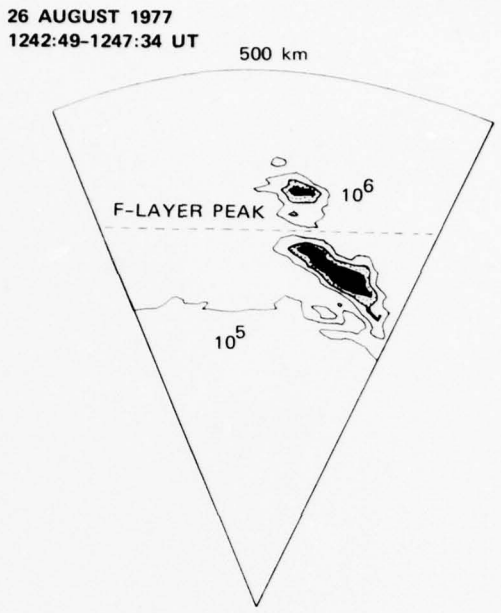

FIGURE 6 CONTOUR MAP OF ALTAIR BACKSCATTER DEPICTING A SPREAD-F STRUCTURE TILTED WEST FROM VERTICAL, AND ITS SPATIAL RELATIONSHIP TO THE PEAK ALTITUDE AND BOTTOMSIDE OF F LAYER

of the magnetic meridian. The altitude of the bottomside of the F layer in this more disturbed example is 270 km, 30 km higher than that in the previous example.

The feature of particular interest in Figure 6 is the tilted, slab-like irregularity region. As discussed in Section V, this map is the first actual confirmation that such geometrical structures exist in the equatorial ionosphere. Its existence, however, has been inferred previously by other less direct means. Its cross-section transverse to geomagnetic field lines (as shown in Figure 6) is 30 by 150 km with a tilt of approximately 45^{o} west of vertical. Note that since the scan is from west to east, a more isotropic backscatter region would have to be drifting eastward and downward at high velocities for the shape to be a temporal effect caused by finite scan time.

Having demonstrated the value of AMTAC scans for determining the spatial distribution of irregularities, their size, shape and orientation, we present a third example that illustrates the value of repeated AMTAC scans for extracting irregularity drift velocity transverse to the geomagnetic field. Four contour maps constructed from sequential AMTAC scans on 26 August 1977 are shown in Figure 7. The ionospheric conditions were more disturbed than in previous examples, as implied by the more widespread presence of backscatter regions. The backscatter intensity is comparable to that in Figure 6. As before, we note that these even more disturbed conditions are associated with a bottomside of the F layer that is higher than those observed in the two previous examples. Here, we have bottomside altitude that is above 300 km, at least 30 km higher than in the previous example and 60 km higher than in the first example.

The irregularity drift velocity can be inferred by scaling the spatial displacement of similar features that appear in succeeding maps and dividing the separation distance by the intermap period. Several features can be identified in the maps in Figure 7, all showing by their displacements to the right in succeeding maps that there is a generally eastward drift. The drift appears to be approximately 60 to 70 m/s. Vertical drift, if present, is small enough that it is not apparent.

We can estimate the range of velocities that can be estimated by this technique if we assume that the lifetimes of these irregularity regions are long enough. For example, at 300-km altitude, the map covers a transverse distance of approximately 300 km. Then for an intermap period of 5 min, we compute maximum east-west velocity of 1 km/s. Since east-west drift velocities are usually of the order of 100 m/s (e.g., Woodman, 1972), all east-west velocities of interest can easily be estimated by this technique, provided that the lifetimes of the irregularities are greater than the intermap period. This seems to be the case if all irregularity regions behave as those in Figure 7. Vertical velocities of interest can also be estimated by this technique provided there is measurable vertical displacement in the structure before it drifts out of the scanned region.

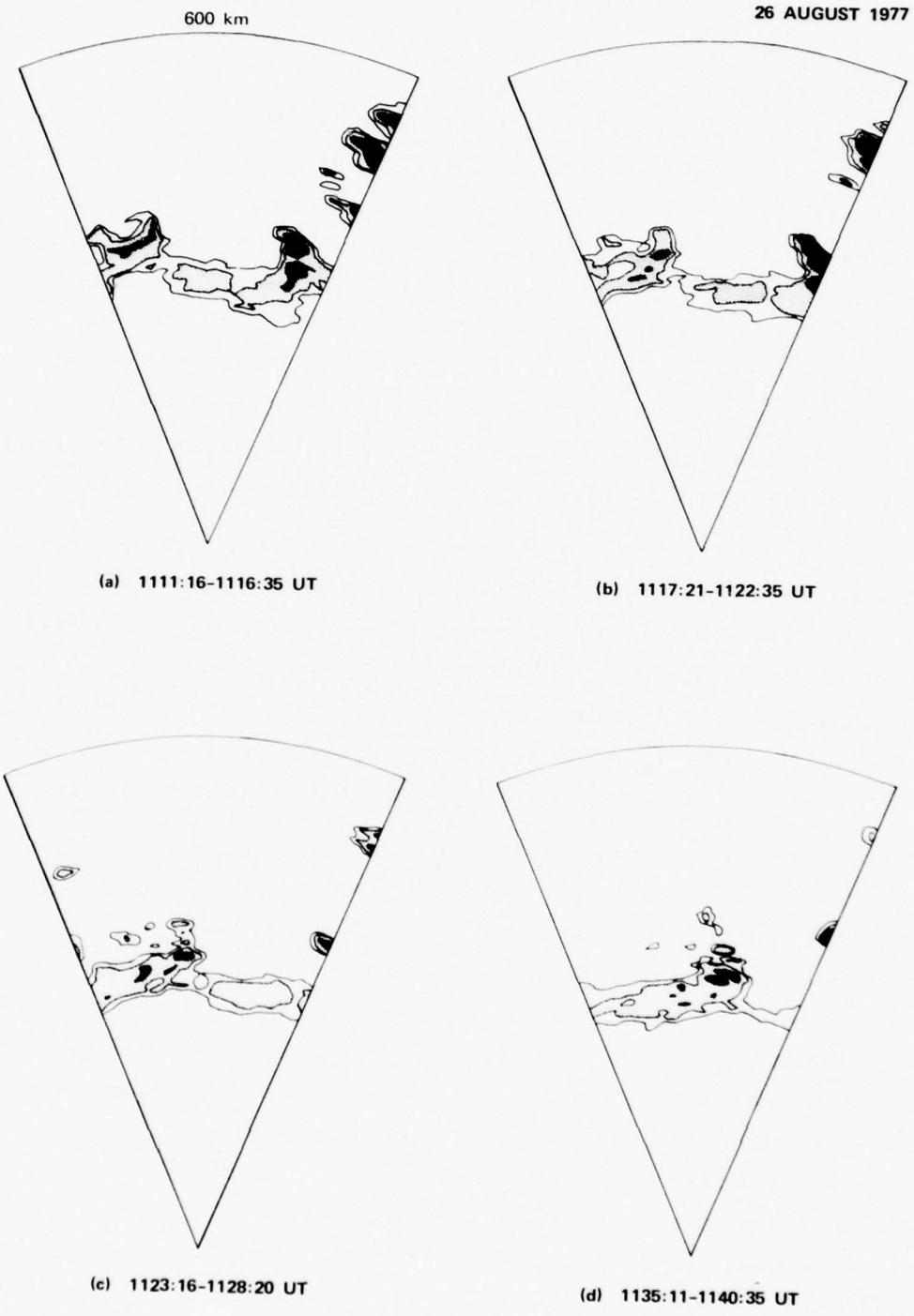

FIGURE 7 SEQUENCE OF AMTAC SCANS SHOWING THE EASTWARD DRIFT OF 1-m SPREAD-F IRREGULARITIES

V. DISCUSSION OF RESULTS

In this section, we discuss the results presented in the previous section in the context of experimental results of other researchers and with the collisional Rayleigh-Taylor instability as the mechanism responsible for equatorial spread-F.

First, it is desirable to "calibrate" the ALTAIR results obtained at 155 MHz with those obtained with the Jicamarca radar at 50 MHz. By calibrate, we mean to establish a relationship between spread-F observations by ALTAIR and by the Jicamarca radar. The differences are presumed to be caused by the wavelength dependence of the spread-F irregularity spectrum. More specifically, we wish to determine whether the backscatter observed with ALTAIR is associated with "weak" or "strong" spread F as seen at 50 MHz with the Jicamarca radar. This association is important since a significant portion of the data base that constitutes our knowledge of equatorial spread-F is derived from Jicamarca radar observations.

Balsley and Farley (1975) have defined "weak" spread F at 50 MHz to be backscatter that is generally less than 20 dB above incoherent-scatter levels. They suggested that weak spread-F echoes are caused by partial reflections from the steep bottomside of the nighttime F layer. In their gradient backscatter model, the received power is found to be proportional to the sixth power of the radar wavelength. If their model is correct, the backscatter intensity at 155 MHz from the same gradient should be 29 dB weaker than that at 50 MHz. By their definition of "weak" spread-F, corresponding backscatter at 155 MHz would be below incoherent-scatter levels. Therefore, until other evidence becomes available to judge otherwise, we interpret all spread-F backscatter observed with ALTAIR to be associated with "strong" spread-F backscatter at 50 MHz. It is of interest in reference to our introductory remarks that "weak" spread-F does not appear to be associated with scintillations at gigahertz frequencies (Basu et al., 1977; Morse et al., 1977).

Another crude comparison can be made between the backscatter intensities observed by the two radars. Farley et al. (1970) state that backscatter at 50 MHz has been observed to reach 70 to 80 dB above incoherent-scatter levels. On the other hand, the highest values published are on the order of 50 dB. From the limited amount of ALTAIR data analyzed thus far, we have seen examples of backscatter that reached 30 dB above incoherent-scatter levels. A 20 dB difference in backscatter intensity would give a wavelength dependence of approximately λ^4. If we use the maximum difference in signal strength of 50 dB, we obtain a wavelength of approximately λ^{10}. Analysis of data collected during simultaneous observations of spread-F backscatter at 155 and 415 MHz with ALTAIR (during the Wideband Equatorial Program) should be useful in obtaining a better estimate of the wavelength dependence of the small-scale irregularities associated with equatorial spread F.

One of the most intriguing features of the disturbed equatorial ionosphere is the existence of "plasma bubbles" that originate in the bottomside of the F layer and appear to "percolate" up through the F-layer peak to the topside (e.g., Hanson and Sanatani, 1973). Plasma bubbles appear to be intimately related to equatorial spread-F, gigahertz scintillations and "plume-like" structures observed in range-time-intensity (RTI) maps made from Jicamarca radar data (Woodman and La Hoz, 1976; McClure et al., 1977). Plasma bubbles are characterized by depletions in electron density by as much as three orders of magnitude below the ambient levels. These plasma bubbles are likely to be depletions of entire geomagnetic flux tubes. There is evidence that radar backscatter occurs from regions of steep electron density gradients presumably associated with the walls of plasma bubbles (Morse et al., 1977), and perhaps also with the depleted regions where highly structured electron density fluctuations have been observed (McClure et al., 1977).

Thus far, we have not observed depleted regions in the electron density profiles obtained from ALTAIR data. Since plasma bubbles are large-scale structures (of the order of 100-km dimension transverse to the geomagnetic field), it is not a question of radar resolution. Instead, it is likely that the backscatter that corresponds to the spread-F

irregularity regions is coincident in space with the plasma bubbles, and that spread-F backscatter is strong enough to fill in any depletions in the electron density profiles that would have been derived from incoherent-scatter. In other words, the absence of depletions in the electron density profiles obtained with ALTAIR may imply that 1-m irregularities are present everywhere within a plasma bubble. It is possible and would be highly profitable to determine whether depletions can be detected with ALTAIR by incoherent scatter when the radar beam is scanned (at significantly off-perpendicular angles to the geomagnetic field) across the same magnetic flux tube that is producing spread-F backscatter.

The generation of rising plasma bubbles is believed to be caused by the collisional Rayleigh-Taylor instability (e.g., Scannapieco and Ossakow, 1976). The instability growth properties are consistent with the observation that spread-F tends to occur when the F layer is at high altitudes. Farley et al. (1970) have reported an altitude threshold for the occurrence of spread F to be greater than 350 km during sunspot maximum and greater than 250 km during sunspot minimum. As described in Section IV, the electron density profiles derived from ALTAIR data are consistent with the results of Farley et al. (1970) and with the theoretical model. We have found that at quiet times the bottomside of the F layer is about 220 km. Higher altitudes have been found to be associated with correspondingly higher spread-F activity. The increase in altitude of the bottomside of the F layer from 220 km to more than 300 km represents a factor of more than two decrease in the ion-neutral collision frequency, a parameter whose inverse value is directly associated with instability growth rate and vertical rise velocity of the plasma bubbles. Ossakow and Chaturvedi (1977) have shown that dramatic increases in both growth rate and vertical bubble velocities can be obtained by decreasing the ion-neutral collision frequency by a factor of two.

With a specified altitude for the bottomside of the F layer and an associated gradient, the Rayleigh-Taylor instability predicts a fixed growth rate. If the perturbations of electron density responsible for the production of plasma bubbles are initiated by thermal fluctuations of the plasma, we would expect plasma bubbles to be uniformly distributed

and to occur at spatial intervals much closer than the observed intervals on the order of 200 km (see Section IV). Clearly, if the initial perturbations are much larger than thermal fluctuations, their spatial and temporal patterns will control the distribution of plasma bubbles.

Examination of published data on plasma bubbles and electron-density depleted regions indicates that they typically are distributed 15 min to an hour in time and 100 to 400 km in horizontal distance. The ALTAIR maps presented in Section IV are consistent with the above observations. In fact, the structure seen in the backscatter maps in Figure 7 is very suggestive of periodic wave structure. It is evident that analyses to understand equatorial spread-F will have to include sources that appear to determine the input scale size and irregularity strength to, for example, the collisional Rayleigh-Taylor instability. Similar conclusions have been reached by Rottger (1973, 1976). Future detailed analysis of ALTAIR data will include an evaluation of various nonthermal sources of periodic perturbations such as traveling ionospheric disturbances (TID).

The question of whether there exists a source that can control the input irregularity scale size and intensity is an intriguing one, and one that is directly relevant to DNA's interests. Clearly, the need for a modulation source that must operate in conjunction with an amplification source (e.g., a plasma instability) to produce the intense irregularities that can disrupt gigahertz communication channels introduces new problems in the proper extrapolation of these results to the nuclear case.

REFERENCES

Balsley, B. B. and D. T. Farley, "Partial Reflections: A Source of Weak VHF Equatorial Spread-F Echoes," J. Geophys. Res., 80, 4735, 1975.

Balsley, B. B., G. Haerendel, and R. A. Greenwald, "Equatorial Spread-F: Recent Observations and a New Interpretation," J. Geophys. Res., 77, 5625, 1972.

Baron, M. and J. Petriceks, "Incoherent Scattering at Perpendicular Intersection with the Earth's Magnetic Field," J. Geophys. Res., 72, 5325, 1967.

Baron, M., R. Tsunoda, J. Petriceks, and H. Kunnes, "Feasibility of an Incoherent-Scatter Radar Aboard the Space Shuttle," Final Report, Contract P.O. G704210, SRI Project 4278, Stanford Research Institute, Menlo Park, CA, March 1976.

Basu, S., J. Aarons, J. P. McClure, C. La Hoz, A. Bushby, and R. F. Woodman, "Preliminary Comparisons of VHF Radar Maps of F-Region Irregularities with Scintillations in the Equatorial Region," (accepted for publication), J. Atmos. Terr. Phys., 1977.

Bowles, K. L., and Staff of Jicamarca Radio Observatory, "Profiles of Electron Density Over the Magnetic Equator Obtained Using the Incoherent Scatter Technique," Tech. Note 169, National Bureau of Standards, March 16, 1963.

Chesnut, W. G., J. C. Hodges, and R. L. Leadabrand, "Auroral Wavelength Dependence Studies," Contract AF 30(602)-3734, SRI Project 5535, Stanford Research Institute, Menlo Park, CA, 1968.

Christiansen, R. M., "Preliminary Report of S-Band Propagation Disturbance during ALSEP Mission Support (November 19, 1969-June 30, 1970)," NASA Report X-861-71-239, Goddard Space Flight Center, Greenbelt, MD, 1971.

Craft, H. D., Jr. and L. H. Westerlund, "Scintillations at 4 and 6 GHz Caused by the Ionosphere," paper presented at AIAA 10th Aerospace Sciences Meeting, San Diego, CA, 1972.

Crampton, E. E., Jr. and W. B. Sessions, "Experimental Results of Simultaneous Measurement of Ionospheric Amplitude Variations of 136 MHz and 1550 MHz signals at the Geomagnetic Equator," NASA Report X-490-71-54, Goddard Space Flight Center, Greenbelt, MD, 1971.

Evans, J. V., "Theory and Practice of Ionosphere Study by Thomson Scatter Radar," Proc. IEEE, 57,496, 1969.

Farley, D. T., "A Theory of Incoherent Scattering of Radio Waves by a Plasma, 4. The Effect of Unequal Ion and Electron Temperatures," J. Geophys. Res., 71, 4091, 1966.

Farley, D. T., "Irregularities in the Equatorial Ionosphere: The Berkner Symposium," Rev. Geophys. Space Phys., 12, 285, 1974.

Farley, D. T., B. B. Balsley, R. F. Woodman, and J. P. McClure, "Equatorial Spread F: Implications of VHF Radar Observations," J. Geophys. Res., 75, 7199, 1970.

Farley, D. T., J. P. Dougherty, and D. W. Barron, "A Theory of Incoherent Scattering of Radio Waves by a Plasma, II. Scattering in a Magnetic Field," Proc. Roy. Soc. London, A, 263, 238, 1961.

Farley, D. T., J. P. McClure, D. L. Sterling, and J. L. Green, "Temperature and Composition of the Equatorial Ionosphere," J. Geophys. Res., 72, 5837, 1967.

Hanson, W. B. and S. Sanatani, "Large Ni Gradients Below the Equatorial F Peak," J. Geophys. Res., 78, 1167, 1973.

Jaye, W. E., W. G. Chesnut, and B. Craig, "Analysis of Auroral Data from the Prince Albert Radar Laboratory," Final Report, Contract 601932 under DA-30-069-AMC-333(Y), SRI Project 7465, Stanford Research Institute, Menlo Park, CA, 1969.

Kelley, M. C., G. Haerendel, H. Kappler, A. Valenzuela, B. B. Balsley, D. A. Carter, W. L. Ecklund, C. W. Carlson, B. Hausler, and R. Torbert, "Evidence for a Rayleigh-Taylor Type Instability and Upwelling of Depleted Density Regions during Equatorial Spread F," Geophys. Res. Lett., 3, 448, 1976.

McClure, J. P., W. B. Hanson, J. H. Hoffman, "Plasma Bubbles and Irregularities in the Equatorial Ionosphere," J. Geophys. Res., 82, 2650, 1977.

McClure, J. P. and R. F. Woodman, "Radar Observations of Equatorial Spread F in a Region of Electrostatic Turbulence," J. Geophys. Res., 77, 5617, 1972.

Morse, F. A., B. C. Edgar, H. C. Koons, C. J. Rice, W. J. Heikkila, J. H. Hoffman, B. A. Tinsley, J. D. Winningham, A. B. Christensen, R. F. Woodman, J. Pomalaza, and N. R. Teixeira, "Equion, an Equatorial Ionospheric Irregularity Experiment," J. Geophys. Res., 82, 578, 1977.

Ossakow, S. L. and P. K. Chaturvedi, "Morphology of Rising Equatorial Spread-F Bubbles," EOS, Trans. AGU, 58, 1202, 1977.

Pineo, V. C., D. P. Hynek, and G. H. Millman, "Geomagnetic Effects on the Frequency Spectrum of Incoherent Backscatter Observed at 425 Megacycles Per Second at Trinidad," J. Geophys. Res., 68, 2695, 1963.

Rottger, J., "Wave-Like Structures of Large-Scale Equatorial Spread-F Irregularities," J. Atmos. Terr. Phys., 35, 1195, 1973.

Rottger, J., "The Macro-Scale Structure of Equatorial Spread-F Irregularities," J. Atmos. Terr. Phys., 38, 97, 1976.

Scannapieco, A. J. and S. L. Ossakow, "Nonlinear Equatorial Spread-F," Geophys. Res. Lett., 3, 451, 1976.

Woodman, R. F., "East-West Ionospheric Drifts at the Magnetic Equator," Space Res., 12, 969, 1972.

Woodman, R. F. and C. La Hoz, "Radar Observations of F Region Equatorial Irregularities," J. Geophys. Res., 81, 5447, 1976.

Appendix

RELATIONSHIP BETWEEN THE MEAN AND THE MEAN OF THE LOGARITHM OF A RAYLEIGH RANDOM VARIABLE

Linear and logarithmic signal detection are two of the most common operations performed on a received signal before it is recorded. If the output signal is recorded without integration, it is possible to directly convert the recorded signal from one form to the other (log to linear, or vice versa). However, very often, the output signal is integrated over several records before recording (e.g., to reduce the data transmission rate or to limit the bulk of the recorded data). In this case, it is not always convenient, even if possible, to convert the recorded average signal from one form to the other. The difficulty arises because the log operation is a nonlinear one. In this Appendix, we derive the relationship between the mean and the mean of the (natural) logarithm of a Rayleigh random variable, x.

The mean value is defined by

$$\bar{x} = \int_{-\infty}^{\infty} x\, p(x)\, dx \quad . \tag{A-1}$$

For a Rayleigh distribution,

$$p(x)\, dx = \frac{x}{\sigma^2}\, e^{-\frac{x^2}{2\sigma^2}}\, dx \quad . \tag{A-2}$$

Therefore,

$$\bar{x} = \int_{0}^{\infty} \frac{x^2}{\sigma^2}\, e^{-\frac{x^2}{2\sigma^2}}\, dx \quad . \tag{A-3}$$

But

$$\int_o^\infty x^{2a}\, e^{-px^2}\, dx = \frac{1 \cdot 3 \cdot 5 \ldots (2a - 1)}{2^{a+1}\, p^a} \sqrt{\frac{\pi}{p}} \qquad \text{(A-4)}$$

Let $a = 1$ and $p = \frac{1}{2\sigma^2}$, then Eq. (A-3) becomes

$$\bar{x} = \sigma \sqrt{\frac{\pi}{2}} \qquad \text{(A-5)}$$

Next, we derive the mean value of the logarithm of a Rayleigh random variable.

$$\overline{\log x} = \int_o^\infty \log x \, \frac{x}{\sigma^2}\, e^{-\frac{x^2}{2\sigma^2}}\, dx \quad . \qquad \text{(A-6)}$$

Let $r = x^2$, $dr = 2x\, dx$. Therefore,

$$\overline{\log x} = \frac{1}{4\sigma^2} \int_o^\infty \log r\, e^{-\frac{r}{2\sigma^2}}\, dr \quad . \qquad \text{(A-7)}$$

But

$$\int_o^\infty e^{-ux} \log x\, dx = -\frac{1}{u}(C + \log u) \qquad \text{(A-8)}$$

where C = Euler's constant.

= .577215 ...

Let $u = \frac{1}{2\sigma^2}$. Therefore,

$$\overline{\log x} = \frac{1}{2} \left[\log (2\sigma^2) - C\right] \quad . \qquad \text{(A-9)}$$

Solving for σ in Eq. (A-9),

$$\log (2\sigma^2) = 2 \overline{\log x} + C$$

$$\sigma = \sqrt{\frac{e^{2 \overline{\log x}} e^{C}}{2}}$$

$$\sigma = K e^{\overline{\log x}} \qquad \text{(A-10)}$$

where $K = \sqrt{\frac{e^{C}}{2}}$

Substituting Eq. (A-10) into Eq. (A-5),

$$\bar{x} = K\sqrt{\frac{\pi}{2}}\, e^{\overline{\log x}} \qquad \text{(A-11)}$$

Therefore, $\bar{x}$ is related to $\overline{\log x}$ by a constant.

Also of interest is the relationship of $\bar{x}$ and $\overline{\log x}$ to $\overline{x^2}$.

$$\overline{x^2} = \int_0^\infty \frac{x^3}{\sigma^2} e^{-\frac{x^2}{2\sigma^2}} dx \quad . \qquad \text{(A-12)}$$

Let $r = \frac{x^2}{2\sigma^2}$, $dr = \frac{x dx}{\sigma^2}$. Therefore,

$$\overline{x^2} = 2\sigma^2 \int_0^\infty r\, e^{-r}\, dr$$

and

$$\overline{x^2} = 2\sigma^2 \quad . \qquad \text{(A-13)}$$

From Eq. (A-5),

$$\overline{x^2} = \frac{4}{\pi} \bar{x}^2 \qquad \text{(A-14)}$$

and from Eq. (A-11)

$$\overline{x^2} = 2K^2 \left(e^{\overline{\log x}} \right)^2 \qquad \text{(A-15)}$$

DISTRIBUTION LIST

DEPARTMENT OF DEFENSE

Assistant Secretary of Defense
Cmd., Cont., Comm. & Intell.
ATTN: J. Babcock
ATTN: M. Epstein

Assistant to the Secretary of Defense
Atomic Energy
ATTN: ATSD (AE)

Director
Command and Control Technical Center
ATTN: C-312, R. Mason
ATTN: C-650, W. Heidig
ATTN: C-650, G. Jones

Director
Defense Advanced Rsch. Proj. Agency
ATTN: Nuclear Monitoring Research
ATTN: Strategic Tech. Office

Defense Communication Engineer Center
ATTN: Code R410, J. McLean

Director
Defense Communications Agency
ATTN: Code 810, R. Rostron
ATTN: Code 480
ATTN: Code 1018
ATTN: M. Raffensperger

Defense Communications Agency
WWMCCS System Engineering Org.
ATTN: R. Crawford

Defense Documentation Center
Cameron Station
12 cy ATTN: TC

Director
Defense Intelligence Agency
ATTN: W. Wittig, DC-7D
ATTN: DT-1B

Director
Defense Nuclear Agency
ATTN: DDST
ATTN: TISI
ATTN: STVL
3 cy ATTN: TITL
3 cy ATTN: RAAE

Commander
Field Command, DNA
ATTN: FCPR

Director
Interservice Nuclear Weapons School
ATTN: Doc. Con.

Director
Joint Strat. Tgt. Planning Staff
ATTN: JLTW-2
ATTN: JPST, CAPT G. Goetz

DEPARTMENT OF DEFENSE (Continued)

Chief
Livermore Division, Field Command, DNA
Lawrence Livermore Laboratory
ATTN: FCPRL

Director
National Security Agency
ATTN: R5
ATTN: F. Leonard
ATTN: J. Skillman
ATTN: P. Clark

OJCS/J-3
ATTN: WWMCCS Eval. Ofc., Mr. Toma

Under Secy. of Defense for Rsch. & Engrg.
ATTN: S&SS (OS)

DEPARTMENT OF THE ARMY

Commander/Director
Atmospheric Sciences Laboratory
U.S. Army Electronics Command
ATTN: DELAS-BL-D, H. Holt
ATTN: DELAS-EO, F. Niles

Director
BMD Advanced Tech. Ctr.
ATTN: ATC-R, D. Russ
ATTN: ATC-T, M. Capps

Program Manager
BMD Program Office
ATTN: DACS-BMT, J. Shea

Chief C-E Services Division
U.S. Army Communications Cmd.
ATTN: CC-OPS-CE

Commander
FRADCOM Technical Support Directorate
ATTN: DRSEL-PL-ENV, H. Bomke
ATTN: DRSEL-NL-RD, H. Bennett

Commander
Harry Diamond Laboratories
ATTN: DELHD-NP, C. Moazed
ATTN: DELHD-TI, M. Weiner
ATTN: DELHD-NP, F. Wimenitz
ATTN: DELHD-RB, R. Williams

Director
TRASANA
ATTN: TCC, F. Payan, Jr.
ATTN: ATAA-SA
ATTN: ATAA-TAC, LTC Hesse

Commander
U.S. Army Comm-Elec. Engrg. Instal. Agy.
ATTN: CCC-EMEO, W. Nair
ATTN: EED-PED, G. Lane

DEPARTMENT OF THE ARMY (Continued)

Commander
U.S. Army Foreign Science & Tech. Ctr.
ATTN: R. Jones
ATTN: P. Crowley

Commander
U.S. Army Materiel Dev. & Readiness Cmd.
ATTN: DRCLDC, J. Bender

Commander
U.S. Army Missile Intelligence Agency
ATTN: J. Gamble

Commander
U.S. Army Missile R&D Command
ATTN: DRDMI-XS, Chief Scientist
ATTN: Chief, Doc. Section

Commander
U.S. Army Nuclear & Chemical Agency
ATTN: Library

Commander
U.S. Army SATCOM Agency
ATTN: Doc. Con.

DEPARTMENT OF THE NAVY

Chief of Naval Operations
ATTN: OP 943, LCDR Huff

Chief of Naval Research
ATTN: Code 461

Commander
Naval Electronic Systems Command
ATTN: PME 117-T, Satellite Comm. Project Off.
ATTN: PME 117
ATTN: NAVALEX 034, T. Hughes

Commanding Officer
Naval Intelligence Support Ctr.
ATTN: STIC 12, Mr. Dubbin

Commander
Naval Ocean Systems Center
ATTN: Code 0230, C. Baggett
ATTN: Code 81, R. Eastman
3 cy ATTN: Code 532, W. Moler

Director
Naval Research Laboratory
ATTN: Code 5460, Electromag. Prop. Br.
ATTN: Code 5465, Prop. Applications
ATTN: Code 2600, Tech. Library
ATTN: Code 5430, Satellite Comm.
ATTN: Code 7730, E. McClean
ATTN: Code 5400, Hq. Comm. Dir., B. Waid
ATTN: Code 7701, J. Brown
ATTN: Code 7700, T. Coffey
ATTN: Code 5410, J. Davis

Commander
Naval Sea Systems Command
ATTN: CAPT Pitkin

Commander
Naval Space Surveillance System
ATTN: CAPT J. Burton

DEPARTMENT OF THE NAVY (Continued)

Naval Space System Activity
ATTN: A. Hazzard

Officer-in-Charge
Naval Surface Weapons Center
ATTN: Code WA501, Navy Nuc. Prgms. Off.

Commander
Naval Surface Weapons Center
Dahlgren Laboratory
ATTN: DF-14, R. Butler

Director
Strategic Systems Project Office
ATTN: NSP-2141
ATTN: NSSP-2722, F. Wimberly

DEPARTMENT OF THE AIR FORCE

Commander
ADCOM/DC
ATTN: DC, Mr. Long

Commander
ADCOM/XPD
ATTN: XPDQQ

AF Geophysics Laboratory, AFSC
ATTN: OPR, A. Stair
ATTN: OPR-1, J. Ulwick
ATTN: LKB, K. Champion
ATTN: PHD, J. Mullen
ATTN: SUOL, Rsch. Library
ATTN: PHP, J. Aarons
ATTN: PHD, J. Buchau

AF Weapons Laboratory, AFSC
ATTN: DYC, Capt L. Wittwer
ATTN: CA, A. Guenther
ATTN: SUL
ATTN: DYC, J. Kamm

AFTAC
ATTN: TF, Maj Wiley

Air Force Avionics Laboratory, AFSC
ATTN: AAD, W. Hunt
ATTN: AAB, H. Hartman
ATTN: AAD, A. Johnson

Headquarters
Electronic Systems Division/XR
ATTN: XRE, Lt Michaels
ATTN: XR, J. Deas

Headquarters
Electronic Systems Division/YSEA
ATTN: YSEA

Commander
Foreign Technology Division, AFSC
ATTN: NICD, Library
ATTN: FTD, B. Ballard

Hq. USAF/RD
ATTN: RDQ

DEPARTMENT OF THE AIR FORCE (Continued)

Commander
Rome Air Development Center, AFSC
ATTN: EMTLD, Doc. Library
ATTN: OCSE, V. Coyne

Commander
Rome Air Development Center, AFSC
ATTN: EEP, A. Lorentzen

SAMSO/MN
ATTN: MNX
ATTN: MNNL, Lt Col Kennedy

SAMSO/SK
ATTN: SKA, Capt Clavin

SAMSO/SZ
ATTN: SZJ, Maj Doan

SAMSO/YA
ATTN: YAT, Capt Blackwelder

Commander in Chief
Strategic Air Command
ATTN: NRT
ATTN: XPFS, Maj Stephan
ATTN: DOK, Chief Scientist
ATTN: ADWATE, Capt Bauer

DEPARTMENT OF ENERGY

EG&G, Inc.
Los Alamos Division
ATTN: Doc. Con. for J. Fu
ATTN: Doc. Con. for J. Walker
ATTN: Doc. Con. for J. Breedlove

University of California
Lawrence Livermore Laboratory
ATTN: Doc. Con. for F. Seward
ATTN: Tech. Info.
ATTN: Doc. Con. for T. Donich

Los Alamos Scientific Laboratory
ATTN: Doc. Con. for R. Taschek
ATTN: Doc. Con. for P. Keaton
ATTN: Doc. Con. for E. Jones
ATTN: Doc. Con. for D. Westervelt
ATTN: Doc. Con. for J. Malik

Sandia Laboratories
ATTN: Doc. Con. for W. Brown
ATTN: Doc. Con. for A. Thornbrough
ATTN: Doc. Con. for 3141, Sandia Rpt. Coll.
ATTN: Doc. Con. for C. Mehl
ATTN: Doc. Con. for J. Martin
ATTN: Doc. Con. for Space Project Div.
ATTN: Doc. Con. for D. Dahlgren
ATTN: Doc. Con. for C. Williams

OTHER GOVERNMENT AGENCIES

Central Intelligence Agency
ATTN: RD/SI, Rm. 5G48, Hq. Bldg. for
OSI/PSTD, Rm. 5, F 19

OTHER GOVERNMENT AGENCIES (Continued)

Institute for Telecommunications Sciences
National Telecommunications & Info. Admin.
ATTN: G. Reed
ATTN: L. Berry
ATTN: W. Utlaut

NASA
Goddard Space Flight Center
ATTN: ATS-6 Ofc., P. Corrigan

National Oceanic & Atmospheric Admin.
Environmental Research Laboratories
Department of Commerce
ATTN: D. Williams
ATTN: R. Grubb
ATTN: C. Rufenach
ATTN: J. Pope

DEPARTMENT OF DEFENSE CONTRACTORS

Aerospace Corporation
ATTN: V. Josephson
ATTN: T. Garfunkel
ATTN: D. Olsen
ATTN: W. Grabowsky
ATTN: T. Salmi
ATTN: J. Carter
ATTN: N. Stockwell
ATTN: G. Anderson
ATTN: SMFA for PWW
ATTN: S. Bower
ATTN: F. Morse
ATTN: F. Bond

Analytical Systems Engineering Corporation
ATTN: Radio Sciences

The Boeing Company
ATTN: D. Murray
ATTN: G. Keister

Brown Engineering Company, Inc.
Cummings Research Park
ATTN: R. Deliberis
ATTN: N. Passino

University of California at San Diego
IPAPS, B-019
ATTN: H. Booker

Charles Stark Draper Laboratory, Inc.
ATTN: J. Gilmore
ATTN: D. Cox

Computer Sciences Corporation
ATTN: H. Blank

COMSAT Laboratories
ATTN: R. Taur

Cornell University
Department of Electrical Engineering
ATTN: D. Farley, Jr.

ESL, Inc.
ATTN: C. Prettie
ATTN: J. Marshall
ATTN: J. Roberts

DEPARTMENT OF DEFENSE CONTRACTORS (Continued)

Ford Aerospace & Communications Corporation
ATTN: J. Mattingley, MS X22

General Electric Company
Space Division
Valley Forge Space Center
ATTN: R. Edsall
ATTN: M. Bortner, Space Sci. Lab.

General Electric Company
ATTN: E. Reibert
ATTN: G. Millman

General Electric Co.-TEMPO
Center for Advanced Studies
ATTN: DASIAC
ATTN: W. Knapp
ATTN: B. Gambill
ATTN: M. Stanton
ATTN: D. Chandler
ATTN: T. Barrett
ATTN: T. Stephans

General Research Corporation
ATTN: J. Garbarino
ATTN: J. Ise, Jr.

Geophysical Institute
University of Alaska
ATTN: N. Brown
ATTN: T. Davis
ATTN: Tech. Library

GTE Sylvania, Inc.
Electronics Systems Grp.-Eastern Div.
ATTN: M. Cross

HSS, Inc.
ATTN: D. Hansen

University of Illinois
Department of Electrical Engineering
ATTN: K. Yeh

Information Science, Inc.
ATTN: W. Dudziak

Institute for Defense Analyses
ATTN: H. Wolfhard
ATTN: F. Bauer
ATTN: J. Aein
ATTN: J. Bengston

Intl. Tel. & Telegraph Corporation
ATTN: Tech. Library

JAYCOR
ATTN: S. Goldman

Johns Hopkins University
Applied Physics Laboratory
ATTN: J. Dassoulas
ATTN: T. Potemra
ATTN: Document Librarian

Kaman Sciences Corporation
ATTN: F. Foxwell
ATTN: B. Bittner

DEPARTMENT OF DEFENSE CONTRACTORS (Continued)

IRT Corporation
ATTN: E. DePlomp

Linkabit Corporation
ATTN: I. Jacobs

Lockheed Missiles & Space Co., Inc.
ATTN: Dept. 60-12
ATTN: D. Churchill

Lockheed Missiles & Space Co., Inc.
ATTN: M. Walt
ATTN: R. Johnson
ATTN: R. Au

M.I.T. Lincoln Laboratory
ATTN: Lib. A-082 for D. Towle
ATTN: Mr. Walden
ATTN: L. Loughlin, Librarian
ATTN: J. Evans
ATTN: D. Clark

Martin Marietta Corporation
Orlando Division
ATTN: R. Heffner

McDonnell Douglas Corporation
ATTN: W. Olson
ATTN: R. Halprin
ATTN: G. Mroz
ATTN: J. Moule
ATTN: N. Harris

Mission Research Corporation
ATTN: S. Gutsche
ATTN: F. Fajen
ATTN: C. Longmire
ATTN: M. Scheibe
ATTN: R. Bogusch
ATTN: P. Fischer
ATTN: R. Kilb
ATTN: R. Hendrick
ATTN: D. Sowle

Mitre Corporation
ATTN: Chief Scientist, W. Sen
ATTN: G. Harding
ATTN: C. Callahan

Pacific-Sierra Research Corporation
ATTN: F. Field, Jr.

Photometrics, Inc.
ATTN: I. Kofsky

Physical Dynamics, Inc.
ATTN: A. Thompson
ATTN: J. Workman

Physical Dynamics, Inc.
ATTN: F. Fremouw

The Trustees of Princeton University
Forrestal Campus Library
ATTN: F. Perkins

Rand Corporation
ATTN: C. Crain
ATTN: E. Bedrozian

DEPARTMENT OF DEFENSE CONTRACTORS (Continued)

R&D Associates
ATTN: E. Gilmore
ATTN: H. Ory
ATTN: B. Gabbard
ATTN: W. Karzas
ATTN: B. Turco
ATTN: R. Lelevier
ATTN: W. Wright, Jr.

Raytheon Company
ATTN: B. Adams
ATTN: G. Thome

Riverside Research Institute
ATTN: R. Popolow

Science Applications, Inc.
ATTN: D. Sachs
ATTN: C. Smith
ATTN: F. Straker
ATTN: J. McDougall
ATTN: D. Hamlin
ATTN: R. Lee
ATTN: L. Linson

Science Applications, Inc.
Huntsville Division
ATTN: D. Divis

Space Data Corporation
ATTN: E. Allen

DEPARTMENT OF DEFENSE CONTRACTORS (Continued)

SRI International
ATTN: R. Leonard
ATTN: R. Leadabrand
ATTN: L. Cobb
ATTN: C. Rino
ATTN: W. Jaye
ATTN: W. Chesnut
ATTN: D. Neilson
ATTN: D. Johnson
ATTN: A. Burns
ATTN: J. Depp
ATTN: G. Smith
ATTN: M. Baron
ATTN: J. Owen
ATTN: R. Tsunoda

System Development Corporation
ATTN: F. Meyer

Technology International Corporation
ATTN: W. Boquist

Tri-Com, Inc.
ATTN: D. Murray

TRW Defense & Space Sys. Group
ATTN: R. Plebuch

Visidyne, Incorporated
ATTN: C. Humphrey
ATTN: J. Carpenter